Palaeogeography, Palaeoclimatology, Palaeoecology 414 (2014) 320–331

Contents lists available at ScienceDirect

Palaeogeography, Palaeoclimatology, Palaeoecology

journal homepage: www.elsevier.com/locate/palaeo

Miocene sedimentary environment and climate change in the northwestern Qaidam basin, northeastern Tibetan Plateau: Facies, biomarker and stable isotopic evidences

Xing Jian [a,1], Ping Guan [a,*], Suo-Tang Fu [b], Dao-Wei Zhang [b], Wei Zhang [a,c], Yong-Shu Zhang [b]

[a] MOE Key Laboratory of Orogenic Belts and Crustal Evolution, School of Earth and Space Sciences, Peking University, Beijing 100871, PR China
[b] Qinghai Oilfield Company, PetroChina, Dunhuang 736202, PR China
[c] Research Institute of Petroleum Exploration & Development, PetroChina, Beijing 100083, PR China

ARTICLE INFO

Article history:
Received 8 April 2014
Received in revised form 28 August 2014
Accepted 12 September 2014
Available online 22 September 2014

Keywords:
Aridity
Oxygen isotope
Lacustrine carbonate
Organic matter
Qaidam basin
Tibetan Plateau

ABSTRACT

Facies, biomarker and stable isotopic records from the Miocene lacustrine sediments in the northwestern Qaidam basin were investigated to reconstruct the Miocene sedimentary environment and climatic history. Three distinct facies can be recognized. These include the following: (1) gray–black laminated mudstone and marlstone, which represent a semi-deep fresh to semi-brackish lake environment; (2) gray, yellowish massive mudstone, marlstone and siltstone; and (3) yellowish massive sandstone, which imply a shallow brackish lake environment. The decreasing C_{27}/C_{31} and $(C_{27}+C_{29})/(C_{31}+C_{33})$ values, the increasing ACL (mean chain length) values of n-alkanes and the vertical evolution of sedimentary environments indicate the overall intensified aridity, which is considered to be an integrated result of high elevation of the Himalaya–Tibetan system, retreat of the Paratethys and global cooling. High fluctuations of the $\delta^{18}O$ values and primary dolomite contents reveal the hydrologically closed paleolake with intermittently open conditions in the study area during middle–late Miocene. The Qaidam basin is suggested to be hydrologically segmented, based on the stable isotopic data comparison between the study area and the northeastern area. The most negative end of the oscillations of the $\delta^{18}O$ values (indicating the minimal evaporation), which likely represents the isotopic ratio of the meteoric water, surprisingly conveys stability in the Shang Youshashan and Shizigou Formations and displays a positive ~2.5‰ shift. This significant shift was probably due to the climatic aridification and air mass changes around 10–8 Ma rather than the global cooling.

1. Introduction

Late Cenozoic climate change in Asia has attracted considerable attention for decades (e.g. Kutzbach et al., 1993; Shi et al., 1999; Wang et al., 1999; An et al., 2001; Graham et al., 2005; Kent-Corson et al., 2009; Heermance et al., 2013). Recently, an increasing number of studies focused primarily on the Miocene aridification in Central Asia and the corresponding driving mechanism (e.g. Dettman et al., 2003; Hough et al., 2011; Miao et al., 2011, 2012, 2013; Zhuang et al., 2011a; Zhang et al., 2012; Song et al., 2014).

Several factors, including the rapid uplift and high elevation of the Tibetan Plateau (e.g. Molnar et al., 1993; An et al., 2001; Dettman et al., 2003), the retreat of the Paratethys and associated variation of land–sea distribution (Ramstein et al., 1997; Zhang et al., 2007b) and the global cooling (e.g. Miao et al., 2012, 2013; Song et al., 2014), are generally suggested to be the potential triggers for the Miocene climatic transition. The dominant factor remains debatable. Dettman et al. (2003) and Hough et al. (2011) investigated the sedimentary carbonate stable isotopes in the Linxia and Xuanhua basins in the northeastern Tibetan Plateau and observed a shift to more arid climate at 12–10 Ma. This climatic shift was further attributed to the topographic growth. Zhuang et al. (2011a) detected a similar stable isotopic evolution history in the eastern Qaidam basin. Their study advocated that the more arid climate was an integrated result of the high elevation of the Tibetan Plateau and the retreat of the Paratethys. By contrast, Miao et al. (2011) and Song et al. (2014) suggested that the global cooling should be the major contributor for the Middle–Late Miocene aridification in the western Qaidam basin.

In addition to these varying arguments, there are disagreements concerning the timing of the aridification. The eolian deposition was well dated to 8–6 Ma on the Chinese Loess Plateau (Liu, 1985; Ding et al., 1998), which was considered to be associated with the desertification in Central Asia. Wang et al. (1999) and Rieser et al. (2009) reported relatively dry climates prevailed in the Pliocene–Pleistocene, whereas Kent-Corson et al. (2009) suggested an increasing aridity during the

* Corresponding author.
E-mail addresses: xing.jian@mail.wvu.edu (X. Jian), pguanl@pku.edu.cn (P. Guan).
[1] Current address: Department of Geology and Geography, West Virginia University, Morgantown, WV 26505, USA.

http://dx.doi.org/10.1016/j.palaeo.2014.09.011
0031-0182/

whole Neogene. Furthermore, chemical weathering study results indicated the increase of aridification and the climate cooling during late Cenozoic (Jian et al., 2013a). These disagreements imply that more work is needed in order to acquire a further understanding of the late Cenozoic climatic evolution.

Climatic variations can influence sedimentary environments, and thus result in changes of facies in sedimentary basins (e.g. Ruskin and Jordan, 2007; Wang et al., 2012). The organic compounds in lake fine-grained deposits, such as lipid biomarkers which can be determined by local climate changes, are regarded as one of the most important indicators to reconstruct paleoclimate and paleoevironment (e.g. Meyers and Benson, 1987; Meyers and Ishiwatari, 1993; Ficken et al., 2000; Xie et al., 2003; Zhou et al., 2005; Bai et al., 2009). Additionally, sediments in lakes can record the hydrology and climate changes through the stable isotopes of sedimentary carbonate, which commonly reflect the isotopic compositions of meteoric or/and lake water (Talbot et al., 1990, 1994; Cerling and Quade, 1993; Leng and Marshall, 2004).

The Qaidam basin, which is a typical high-altitude terrestrial sedimentary basin, lies in the northeastern sector of the Tibetan Plateau (Fig. 1A). It preserves an exceptionally thick Mesozoic and Cenozoic

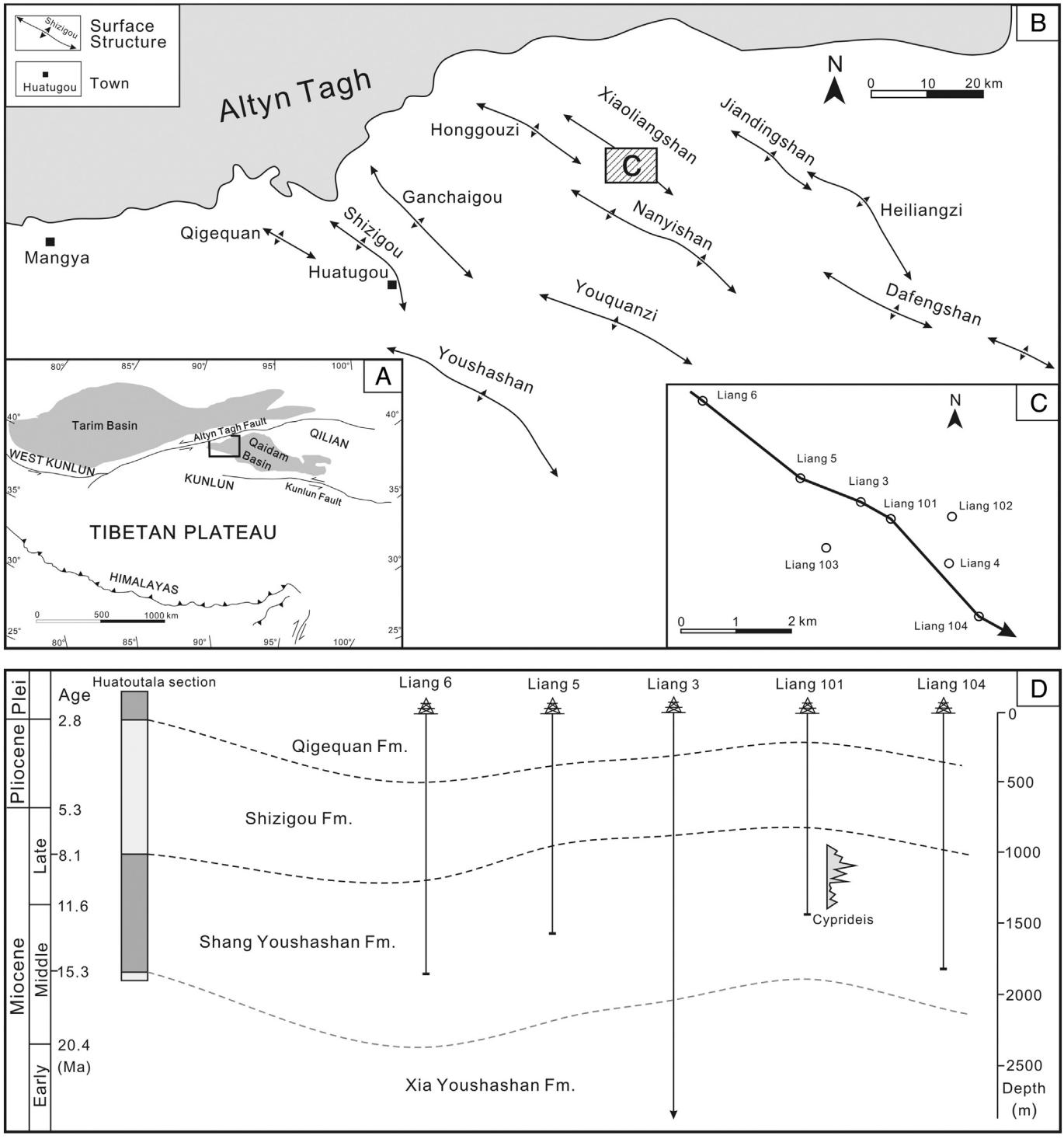

Fig. 1. Geologic settings and stratigraphy of the study area. (A) and (B) The tectonic location of the Qaidam basin and Xiaoliangshang area; (C) Well locations in the Xiaoliangshan area; (D) Subsurface stratigraphy of the drilling wells.

sedimentary succession, with an average thickness up to 8 km (Xia et al., 2001; Jian et al., 2013a,b). The northwestern Qaidam basin (Fig. 1B) is selected as the study area because of the Miocene mixed carbonate–siliciclastic lacustrine deposits here (Jian, 2013), which are very sensitive to the environmental and climatic variations.

In this study, we focus on the Miocene sediments in the Xiaoliangshan area, northwestern Qaidam basin (Fig. 1), and primarily present facies, biomarker and stable isotopic data and the corresponding interpretations. The objectives are to: 1) provide additional climatic indicator data from the subsurface sedimentary rocks in the Qaidam basin; 2) reconstruct the Miocene sedimentary environment evolution and climatic history in the northwestern Qaidam basin; and 3) investigate the principal mechanism for the aridification.

2. Geologic setting and stratigraphy

The rhomb-shaped Qaidam basin lies in the northeastern Tibetan Plateau (Fig. 1A) and covers approximately 120,000 km^2. It contains a thick Mesozoic to Cenozoic continental sedimentary succession. The surface of the basin sits about 2.7–3 km above sea level. The Qaidam basin is bounded by three large mountain ranges which stand up to 5 km above sea level. To the south are the Eastern Kunlun Mountains. The Qilian Mountains are along the east, as a fold-thrust belt of ~300 km wide (Gehrels et al., 2003a,b; Yin et al., 2008a). The Altun Mountains are to the northwest, and the Alytn Tagh Fault is an active left-lateral strike–slip fault (Yue and Liou, 1999; Yin et al., 2002; Yue et al., 2003), which separates the Qaidam basin from the Tarim basin.

The current Qaidam basin is regarded as the result of a convergent system in the northeastern Tibetan Plateau (Tapponnier et al., 2001; Yin et al., 2008b). The structural evolution of the basin is closely linked with the continuous convergence between the Indian and Eurasian plates (Yin and Harrison, 2000; Yin et al., 2008a). A series of thrust fold belts with NW–SE direction are present inside the basin (Fig. 1B) and reverse faults are developed along Qilian Mountains and Kunlun Mountains. The Xiaoliangshan area is located in the northwestern Qaidam basin. It is tightly situated next to the Altun Mountains to the north (Fig. 1B). There are abundant hydrocarbon resources trapped in the shallow subsurface sedimentary strata, and several exploration wells have been drilled (Fig. 1C).

The Qaidam basin has been internally drained since at least late Oligocene, according to the sedimentary facies relationships, provenance, sediment-dispersal paths and isopach relationships (Hanson, 1999; Yin et al., 2002, 2008b). The Miocene sediments of the Qaidam basin were deposited mainly in a fluvial-lacustrine sedimentary environment (Xia et al., 2001; Lu and Xiong, 2009; Zhuang et al., 2011b; Jian, 2013; Song et al., 2014). The Miocene strata contain three stratigraphic units (Fig. 1D), including (1) Xia Youshashan Formation (XYFm., ~22–~15 Ma); (2) Shang Youshashan Formation (SYFm., ~15–~8 Ma); and the lower part of (3) Shizigou Formation (SFm., ~8–2.8 Ma).

3. Materials and methods

More than 400 m rock cores were collected from several hydrocarbon exploration wells (Fig. 1C–D, e.g. Wells Liang 3 and Liang 101). Depth corrections for the rock cores were conducted on the base of well logging data. The rock cores were visually described and graphic sedimentary logs were made for facies analysis and interpretation. More than 60 samples were collected and further made to thin sections for petrography.

Five samples were selected for organic geochemical analysis. The detailed analytical procedures were given in Zhou et al. (2005) and Duan et al. (2011). The air-dried samples were first crushed and then powdered to 100–200 mesh. Soluble organic matters were Soxhlet-extracted with chloroform for 56 h. Then the extracts were filtered and evaporated to dryness, and separated into saturated hydrocarbons, aromatic hydrocarbons and non-hydrocarbon by column chromatography on alumina over silica gel. The saturated hydrocarbons were directly analyzed using a Hewlett-Packard (HP) 6890 gas chromatograph with an HP-5 fused silica capillary column and a HP 5973 mass spectrometer. The operating conditions were: temperature ramped from 80 °C to 290 °C at 3 °C/min and held at 290 °C for 30 min, with He as carrier gas, and the ionization energy of the mass spectrometer was set to 70 eV.

In order to obtain the original isotopic signature of lacustrine primary carbonates, marlstones and calcareous mudstones mainly composed of micritic carbonates (Fig. A1, in Appendix 2) were preferred for carbon and oxygen isotopic analyses. This means that samples with carbonate lithic fragments (i.e. detrital carbonates) and/or diagenetic carbonates were avoided. Twenty-nine samples were selected under microscope, based on the petrographic study (e.g. Fig. A1). The samples (powders) were reacted with 100% phosphoric acid under vacuum and steady at 50 °C for 24 h. The Finnigan MAT-253 mass-spectrometer was used to analyze the contamination-free carbon dioxide gas collected from the reaction. The isotopic results are reported using standard delta (δ) notation with respect to VPDB (Vienna Peedee belemnite). Analytical precision is better than $\pm 0.1‰$ (1σ) for both $\delta^{13}C$ and $\delta^{18}O$ values. Eight samples which had carbon and oxygen isotopic values were also selected for X-ray diffraction (XRD) analysis. The XRD analysis was carried out by using the D/max-rA rotating anode X-ray diffractometer (12 KW) made by Rigaku. Each sample was continuously scanned under 40 kV, 100 mA, wave length of 1.5406, 2θ range of 3°–75°, step width of 0.02° and scanning speed of 4°/min.

4. Results

4.1. Facies

Based on sedimentary structures and lithology, three distinct facies can be recognized in the Miocene strata, i.e., gray–black laminated mudstone and marlstone (Facies 1); gray, yellowish massive mudstone, marlstone and siltstone (Facies 2) and yellowish massive sandstone (Facies 3). The major features of each facies are stated as follows.

4.1.1. Facies 1: gray–black laminated mudstone and marlstone

Facies 1 is characterized by dark gray to black mudstone and marlstone and evident horizontal millimeter-scale laminae (Fig. 2A–B). The lamination is commonly demonstrated by alternating very thin organic- (and clay-) rich muds and fine quartz-rich silts or micritic carbonates (Fig. 2C–D). The boundaries between laminae are generally clear. It is remarkable that there are a great number of coccoid, botryoid and fabaceous pyrite nodules in some mudstones and marlstones (Fig. 2E). XRD analysis results indicate that the sediments are mainly composed of quartz, carbonate (calcite and/or dolomite) and clay minerals and subordinate feldspar, pyrite, gypsum and halite. Fractures are always present in marlstones and mudstones with high carbonate contents. Facies 1 is predominantly present in the Shang Youshashan Formation, and occasionally in the Shizigou Formation.

4.1.2. Facies 2: gray, yellowish massive mudstone, marlstone and siltstone

The significant features of Facies 2 (Fig. 3A–B) are the shallowing colors, the absent laminations and the increasing silty contents. Centimeter-size anhydrite and gypsum crystals, organism burrows and plant remains (probably plant leaves and roots) are often present in this facies (Fig. 3C–D). Facies 2 has the similar mineral composition with Facies 1. It can be seen mainly in the Shizigou Formation and the upper part of the Shang Youshashan Formation.

4.1.3. Facies 3: yellowish massive sandstone

The coarser sediments in this facies are different from Facies 1 and 2 (Fig. 4A). The sandstone layers are relatively thin (less than 1 m) and occasionally present in the study area. Facies 3 are mainly composed of fine sandstones with subordinate medium sandstones. Detrital

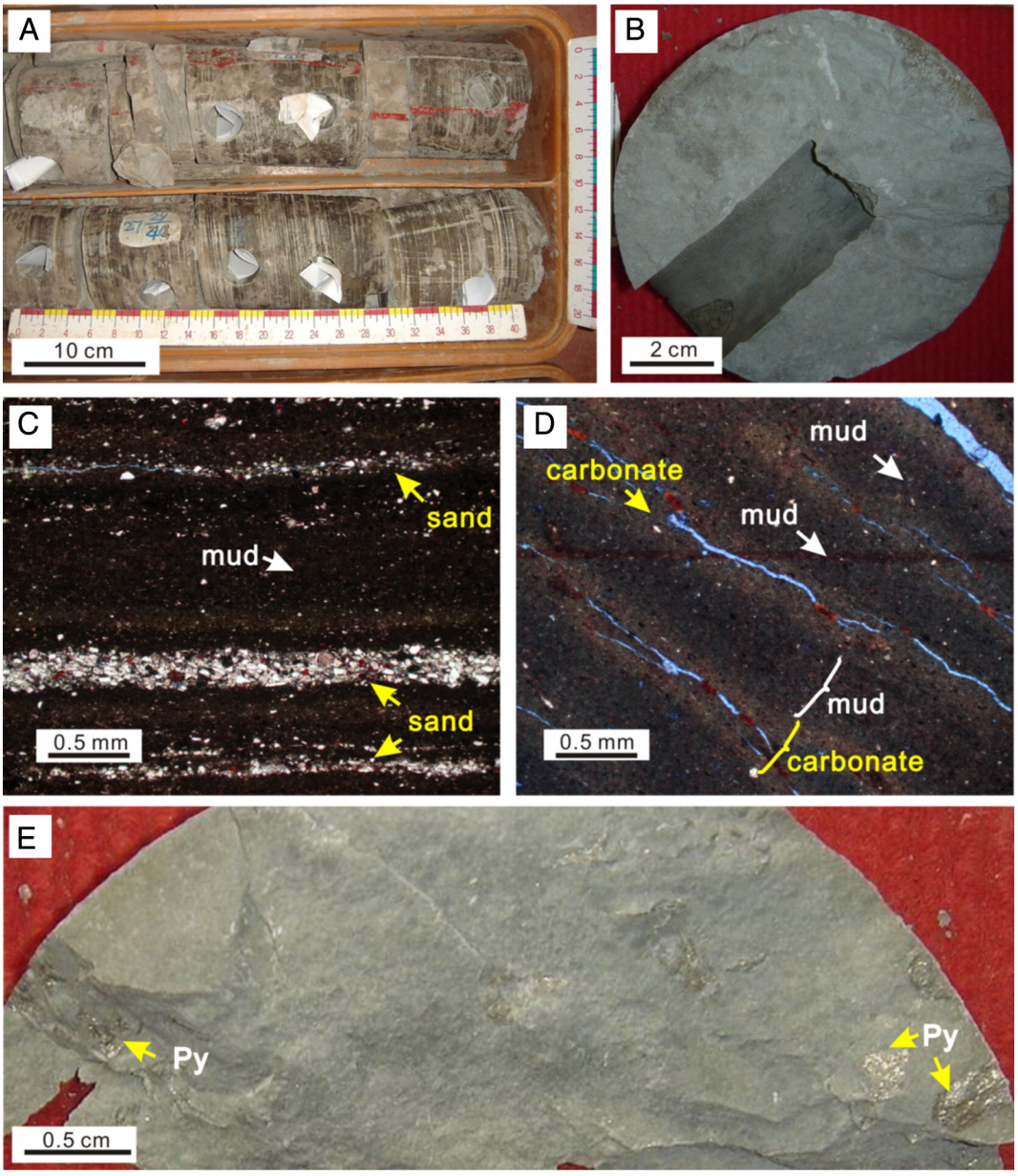

Fig. 2. Photographs and micrographs of major features in Facies 1 (gray–black laminated mudstone). (A) Macroscopic view of the well-developed horizontal laminated mudstone, with the depth of 1363 m–1365 m; (B) gray marlstone (1382.5 m); (C) and (D) Horizontal laminae in the gray–black mudstones, composed of muds and sands (C, 1292 m) or carbonates (D, 1239 m); (E) Pyrite nodules (indicated by yellow arrows) in the gray–black marlstones (Well Liang 6, 1665.7 m). (For interpretation of the references to color in this figure legend, the reader is referred to the web version of this article.)

framework grains are mainly rounded in shape and show relatively well sorting (Fig. 4B–C), with the mean grain sizes up to medium grade. Abundant anhydrite and gypsum crystals are present in these sandstones as matrixes (Fig. 4B). Facies 3 only occurs in the Shizigou Formation.

4.2. n-Alkane distribution and the biomarker proxies

Lipid biomarker analysis results indicate that the n-alkanes of the analyzed samples distribute from C_{14} to C_{35}. They are dominated by the C_{16} or C_{22} homologues. In this study, we use 5 biomarker proxies to interpret the sedimentary environment and climate change, i.e. $(C_{27} + C_{29})/(C_{31} + C_{33})$, C_{27}/C_{31}, CPI, ACL (Poynter et al., 1989) and Paq (Ficken et al., 2000). The calculation and results are shown in Table 1 and Fig. 5. The analyzed samples have $(C_{27} + C_{29})/(C_{31} + C_{33})$ and C_{27}/C_{31} values ranging from 1.2 to 3.5 and from 0.95 to 2.7 (Table 1), respectively, which indicate relatively high proportion of C_{27} and C_{29}. The Paq values, which are between 0.5 and 0.74 (Table 1), suggest relatively dominant C_{23} and C_{25} compared with C_{29} and C_{31}. The CPI values, which indicate the carbon preference of n-alkanes, range from 0.91 to 1.30.

4.3. Carbon and oxygen isotopes of lacustrine carbonate

The stable isotopic data are given in Table 2, and the correlation between $\delta^{13}C$ and $\delta^{18}O$ is illustrated in Fig. A2 (see Appendix 2). The results show that the analyzed samples have obviously large ranges of carbon and oxygen isotopic compositions. The $\delta^{13}C$ and $\delta^{18}O$ values of 21 Shang Youshashan Formation samples vary from −5.4 to 1.9‰ (averaging −1.1‰), from −6.7 to 3.7‰ (averaging −2.5‰), respectively, while the $\delta^{13}C$ and $\delta^{18}O$ values of 8 Shizigou Formation samples have ranges varying from −2.5 to 0.8‰ (averaging −0.5‰), from −4.2 to 0.7‰ (averaging −2.2‰) (Table 2), respectively. The $\delta^{13}C$ and $\delta^{18}O$ values show slightly negative correlation for all of the analyzed

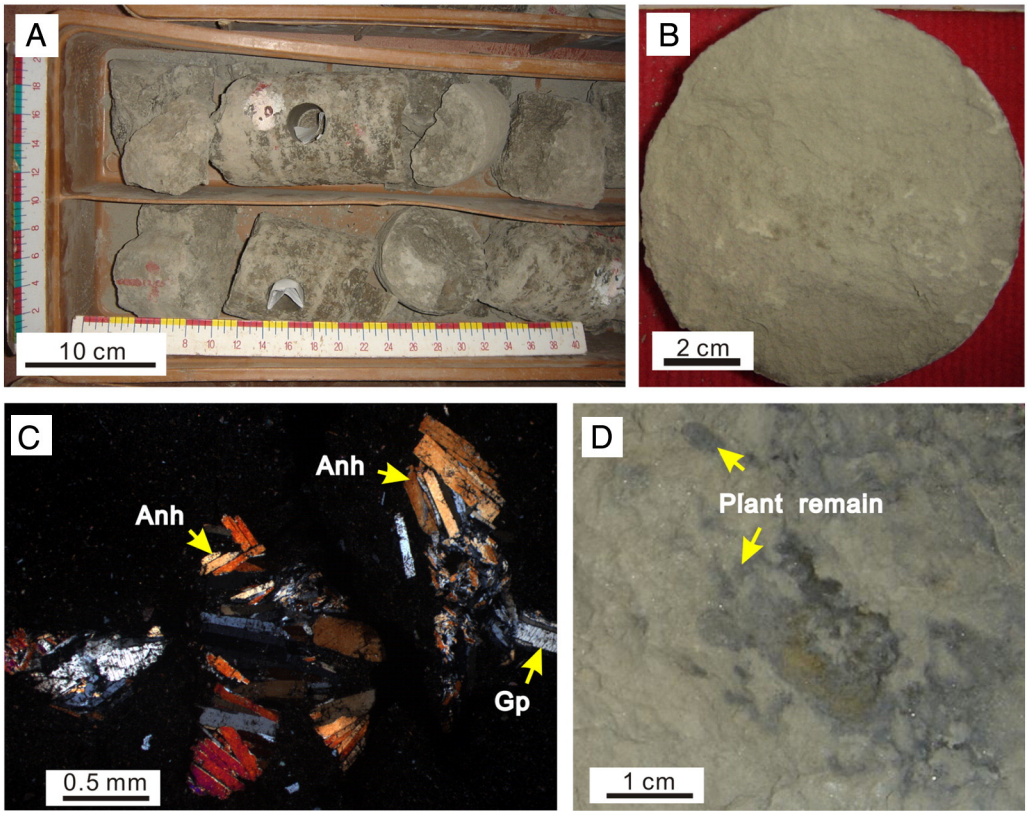

Fig. 3. Photographs and micrographs of major features in Facies 2 (gray, yellowish massive mudstone, marlstone and siltstone). (A) Macroscopic view of the yellowish massive mudstone (736 m–738 m); (B) Yellowish siltstone (783 m); (C) Centimeter-size gypsum and anhydrite crystals (yellow arrows) in mudstone (761 m); (D) Plant remains (indicated by yellow arrows) in mudstone (742 m). (For interpretation of the references to color in this figure legend, the reader is referred to the web version of this article.)

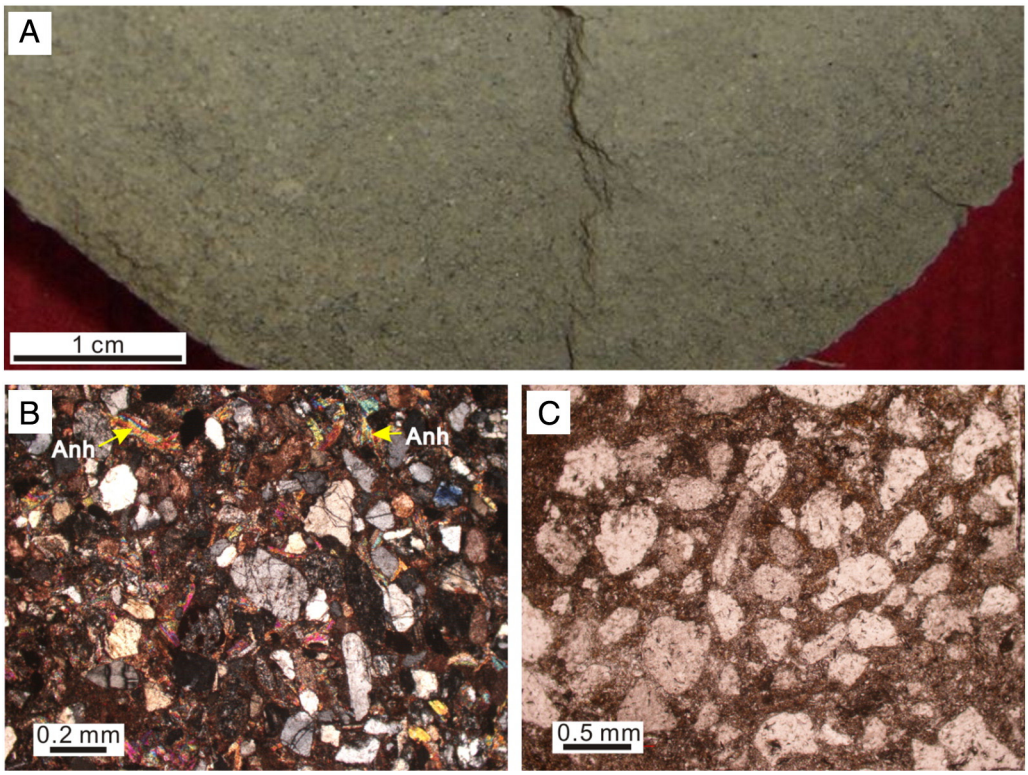

Fig. 4. Photographs and micrographs of major features in Facies 3 (yellowish massive sandstone). (A) Yellowish sandstone (793 m); (B) Fine-medium sandstone with abundant anhydrite (yellow arrows) matrix (792); (C) Medium sandstone composed of subrounded or rounded grains (791 m). (For interpretation of the references to color in this figure legend, the reader is referred to the web version of this article.)

Table 1
Biomarker data of the middle–late Miocene lake sediments in the northwestern Qaidam basin.

Sample	Well	Formation	Biomarker proxies				
			$(C_{27} + C_{29})/(C_{31} + C_{33})$	C_{27}/C_{31}	ACL	Paq	CPI
L101-35	Liang 101	SFm.	1.83	1.54	29.3	0.61	0.98
L101-28	Liang 101	SFm.	1.41	0.95	29.5	0.51	1.30
L101-25	Liang 101	SYFm.	1.98	1.70	29.2	0.65	0.92
L101-10	Liang 101	SYFm.	1.26	0.98	29.5	0.51	1.11
L101-05	Liang 101	SYFm.	2.16	1.79	29.2	0.64	0.91
K2-2*	Kai 2	SYFm.	3.43	2.71	28.7	0.74	0.99
L3-1*	Liang 3	SYFm.	2.72	2.41	29.0	0.69	0.88

SFm. = Shizigou Formation; SYFm. = Shang Youshashan Formation. ACL = $(27*C_{27} + 28*C_{28} + \ldots + 33*C_{33})/\Sigma C_{27-33}$ (Poynter et al., 1989). Paq = $(C_{23} + C_{25})/(C_{23} + C_{25} + C_{29} + C_{31})$ (Ficken et al., 2000). CPI = ΣC_{23-33} (odd)/ΣC_{22-32} (even). All of the proxies are calculated from n-alkane concentrations.
The data with asterisk are from He et al. (2008).

samples, in other words, most samples with high $\delta^{18}O$ values have relatively low $\delta^{13}C$ values (Fig. A2).

5. Interpretation and discussion

5.1. Sedimentary environment

The representative features of the facies suggest that the Xiaoliangshan area was in a lake environment during middle–late Miocene. The lake sedimentary environment is also illustrated by the natural gamma-ray (GR) well log of Well Liang 101, which shows zigzag vertical line in shape (Fig. 6). This interpretation is also supported by unpublished seismic data. The gray–black, yellowish colors and the inexistence of thick and coarse siliciclastic sediments reveal a generally underwater environment. The lake sedimentation had three remarkable features: underdeveloped drainages and low input of clastic detritus, low-energy hydrodynamic conditions and relatively high salinity in some intervals.

Facies 1 is interpreted as deposited in a semi-deep fresh to semi-brackish lake environment (Fig. 6B). The combination of dark colors, abundant clays and well-developed horizontal millimeter-scale-laminations indicate stagnant deep-water conditions. This can be explained as the following: (1) Abundant horizontal laminations, high clay mineral contents and micritic carbonate (Fig. 2) suggest that the mudstones and marlstones were generated in quiet or low-energy hydrodynamic environments; (2) The gray–black mudstones and the occurrence of the pyrite nodules (Fig. 2E, always explained as a production of bacterial activity under deep subaqueous settings) demonstrate reducing environments (Schieber, 2002); (3) the existence of marlstone intervals with relatively abundant primary lacustrine dolomite indicates high salinity of the lake water (Last, 1990).

It is suggested that Facies 2 and 3 were deposited in a shallow brackish lake environment (Fig. 6B). This can be explained as the following: (1) the light gray and yellowish colors (e.g. Fig. 3) and the lack of pyrite nodules indicate an enhanced oxidation condition, which probably resulted from shallowing lake water; (2) the obvious massive structure with subordinate microscopic wavy beddings suggests that these sediments were likely deposited in a relatively higher-energy hydrodynamic water condition (actually the hydrodynamic condition was also low). It is also demonstrated by the common siltstone and sandstone layers (i.e. Facies 3, Fig. 4); (3) the occurrence of plant remains (e.g. Fig. 3D) and vertical organism burrows further reveals a shallow water environment. Furthermore, abundant primary dolomite, anhydrite, gypsum (Figs. 3–4) and halite nodules (or crystals) in mudstones and sandstones imply high salinity in the lake, nevertheless, the absence of halite or gypsum layers indicates that the water was not saline enough to generate evaporite layers at the brine–sediment interface (Lowenstein and Hardie, 1985). Facies 3 is preferred to be regarded as the result of shallow lake environments rather than fluvial or alluvial fan environments, because the architecture of fluvial successions (i.e. channel and

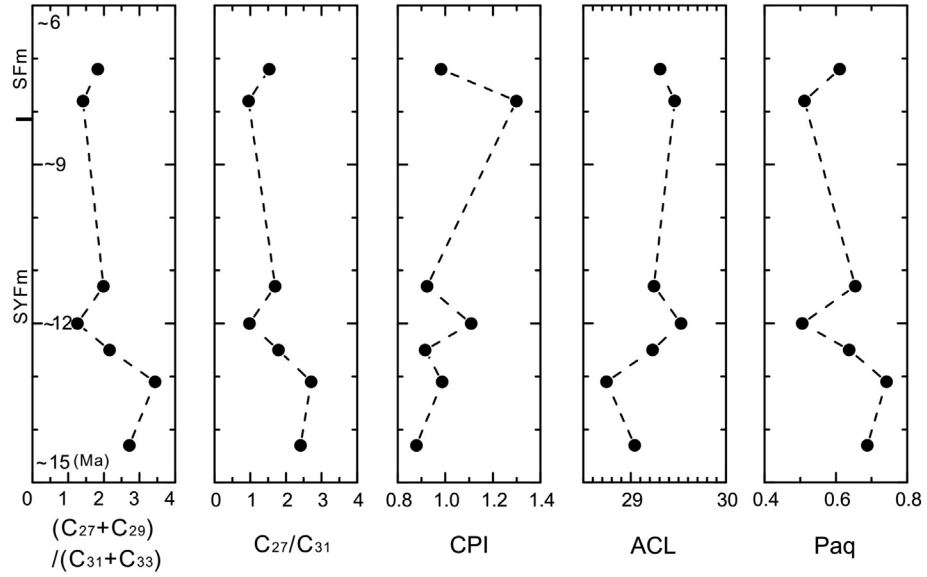

Fig. 5. The vertical series of five biomarker proxies for the lake sediments. The sedimentary ages are estimated based on the sample locations in the stratigraphic intervals. For the ratios, see Table 1.

Table 2
Stable isotopic results of the lacustrine primary carbonate in the northwestern Qaidam basin.

Sample	Formation	$\delta^{13}C$ (V-PDB, ‰)	$\delta^{18}O$ (V-PDB, ‰)
L101-43	SFm.	0.8	−1.7
L101-41	SFm.	−1.0	−3.8
L101-39	SFm.	0.8	−1.5
L101-38	SFm.	−0.6	0.7
L101-35	SFm.	−0.7	−3.5
L101-34	SFm.	−0.5	−3.8
L101-32	SFm.	−0.5	−4.2
L101-28	SFm.	−2.5	−0.1
L101-26	SYFm.	−4.3	3.7
L101-23	SYFm.	0.2	−7.0
L101-22	SYFm.	−0.6	−1.2
L101-21	SYFm.	1.0	−0.7
L101-19	SYFm.	−1.4	−6.1
L101-18	SYFm.	−3.8	0.7
L101-17	SYFm.	−2.3	−1.9
L101-16	SYFm.	0.6	−3.5
L101-14	SYFm.	1.5	−6.6
L101-12	SYFm.	−1.0	−4.1
L101-11	SYFm.	−2.2	−1.7
L101-10	SYFm.	−0.1	−1.2
L101-08	SYFm.	−1.7	−3.7
L101-07	SYFm.	−1.1	−1.1
L101-05	SYFm.	0.0	−1.8
L101-04	SYFm.	1.2	−0.7
L101-01	SYFm.	−1.8	−6.7
L5-1	SYFm.	1.9	−4.3
L6-6	SYFm.	−1.2	−5.3
L6-4	SYFm.	−2.2	−1.4
L6-1	SYFm.	−5.4	1.1

SFm. = Shizigou Formation; SYFm. = Shang Youshashan Formation.

overbank deposits and erosion surfaces between them) cannot be seen in the rock cores, and these sandstone layers are relatively thin and fairly fine in grain size (Fig. 4). Additionally, the vertical distribution of GR well log also reinforces this interpretation (Fig. 6).

Based on the drilling core of Well Liang 101 (Fig. 6A), the sedimentary environment evolution in the Xiaoliangshan area is discussed in this study. The vertical distribution of the facies shows that the Shang Youshashan Formation strata are mainly composed of Facies 1, while the Facies 2 and 3 are predominantly distributed in the Shizigou Formation strata. This implies that the lake water became increasingly shallow and brackish over time during middle–late Miocene. The conclusion can be reinforced by the chloridion analysis result, which shows the sediments in the Shizigou Formation have much higher chloridion contents than the sediments in the Shang Youshashan Formation (unpublished data).

The Paq values of the n-alkanes also support the feature of underdeveloped drainages and low input of terrestrial components and the upward-shallowing lake water. Previous studies have found that emergent and terrestrial plants generally display the predominance of $>C_{27}$, whereas submerged/floating aquatic plants are usually characterized by the predominance of C_{21}, C_{23} or C_{25} (Barnes and Barnes, 1978; Cranwell, 1984; Viso et al., 1993; Ficken et al., 2000). $Paq = (C_{23} + C_{25})/(C_{23} + C_{25} + C_{29} + C_{31})$ based on the n-alkane data (Fig. 5), which was proposed for evaluating the contribution of submerged/floating aquatic macrophyte to the lake sediment organic matter (Ficken et al., 2000). It is suggested that $Paq < 0.1$ corresponds to terrestrial plants, 0.1–0.4 to emergent macrophytes and 0.4–1 to submerged/floating macrophytes (Ficken et al., 2000). In some case studies, a given Paq value would reflect a particular mixture of inputs from two or more of these sources. All of the Paq values of the samples in this study are more than 0.4 (Table 1, Fig. 5), indicating the dominant contribution of submerged/floating macrophytes and very low input of terrestrial plants. This probably means relatively deep lake water and underdeveloped drainages around the Xiaoliangshan area. Besides, the Paq values display a decreasing trend over time (the Paq values of the samples from the Shang Youshashan and Shizigou Formations average in 0.65 and 0.56, respectively), which indicates the increasing input of terrestrial plants and emergent macrophytes, and indirectly supports shallowing lake water environments.

5.2. Paleolake hydrology

In most temperate and high-latitude regions, micritic carbonates (primary carbonates) is commonly considered to be directly precipitated within the surface water of the lake in late spring through summer (Teranes and McKenzie, 2001), when the temperatures are at their warmest and the saturation conditions of the lake culminate (Drummond et al., 1995). The oxygen isotopic composition of micritic carbonate is generally used as a proxy for the oxygen isotopic composition of lake water (Talbot, 1990; Hodell et al., 1998), while carbon isotopes reflect the biologic productivity of a lake (Talbot, 1990). Previous studies have shown that the $\delta^{18}O$ and $\delta^{13}C$ values of lacustrine micritic carbonate can be influenced by temperature, meteoric precipitation, evaporation and the carbon cycle (Talbot, 1990; Leng and Marshall, 2004). Therefore, the carbon and oxygen isotopic data of lacustrine micritic carbonate can be used to evaluate the paleolake hydrology.

Lakes can be divided into two distinct hydrological types: open lake and closed lake. The open lake often occurs in the conditions with high precipitation/evaporation ratios or with sufficient groundwater supply, where the meteoric water has a very short residence time in the lake. In these conditions, the oxygen isotopes of lacustrine micritic carbonate can represent the oxygen isotopes of meteoric water, and generally have very small ranges of variation (or relatively invariant) within a certain period of time (Leng and Marshall, 2004). These variations are normally attributed to the variations in temperature or the isotope composition of precipitation. In contrast, closed lake, which commonly presents in the environments with low precipitation/evaporation ratios or with insufficient groundwater supply, lose water mainly through evaporation, and precipitate carbonate with variable and generally high $\delta^{18}O$ values. The fluctuations in the oxygen isotope composition are mainly a function of long-term changes in the precipitation/evaporation ratio (Leng and Marshall, 2004). The correlation between $\delta^{13}C$ and $\delta^{18}O$ values is often used to estimate the degree of hydrological closure of a lake through time (Talbot, 1990, 1994). Talbot (1990) proposed that carbonates from hydrologically open lakes show little or no correlation between $\delta^{13}C$ and $\delta^{18}O$ values, whereas the correlation would be very high ($r > 0.7$) in closed lake systems. Several studies realized that this interpretation is generally only true for lakes that have attained hydrological closure over extended time frames (Drummond et al., 1995; Li and Ku, 1997). In addition, paleolake hydrology can be evaluated on the base of primary carbonate mineralogy. In freshwater systems (i.e. hydrologically open lakes), calcite usually forms but with increasing evaporation other carbonate minerals can be produced, such as high-Mg calcite, aragonite and dolomite (Talbot and Kelts, 1986).

In this study, the $\delta^{18}O$ values of analyzed micritic carbonates are highly variable, with the variation range over 6‰ (Table 1, Fig. A2), implying predominant closed lake conditions during middle–late Miocene. This can be explained as follows. The variations should not be due to the seasonal temperature changes, because each sample may provide an integrated isotope composition for the lake waters of 10 or even 100 years, depending on the sedimentation rate. And the causes from diagenesis and detrital carbonates can be excluded since we selected the micritic carbonates as the analyzed samples. Hence, the high variations in $\delta^{18}O$ values can be attributed to variable meteoric precipitation and evaporation. If we assume the oxygen isotopes of meteoric water are relatively constant within a relatively short period, the samples with high $\delta^{18}O$ values should be precipitated in intensive evaporation lake environments, in contrast, the low $\delta^{18}O$ values imply mild evaporation conditions. The conclusion is reinforced by our XRD analysis results. The samples with high $\delta^{18}O$ values have high dolomite and low calcite contents (Fig. 7), indicating the occurrence of intensive evaporation.

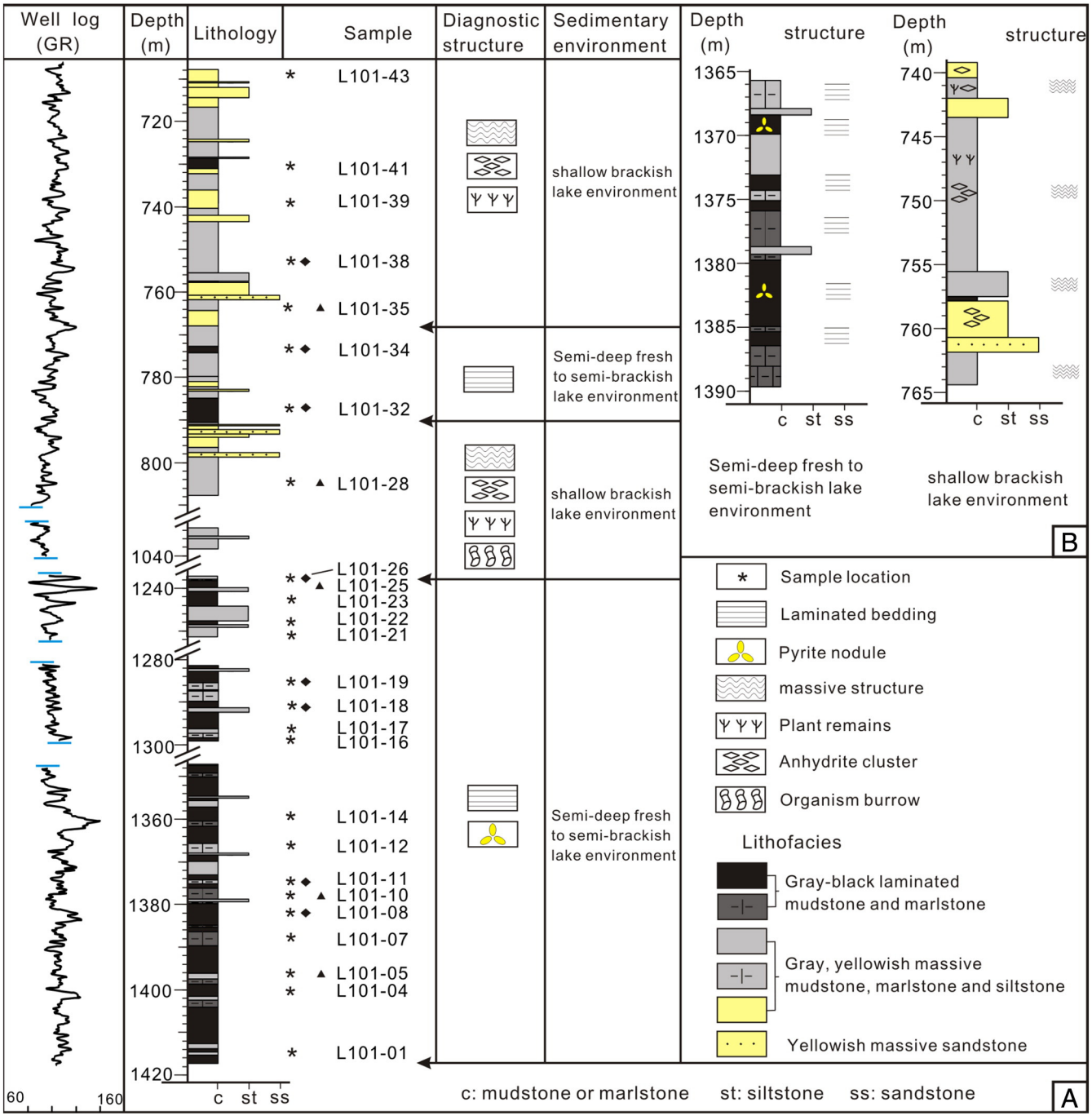

Fig. 6. (A) Facies vertical variation, diagnostic structure distributions and corresponding sedimentary environment interpretations of drilling core of Well Liang 101 in the Xiaoliangshan area. (B) Representative assemblages of facies representing different sedimentary environments. Note that the locations of samples for analysis are shown.

However, the correlation plot between $\delta^{13}C$ and $\delta^{18}O$ values displays poor covariance for the analyzed samples (Fig. A2), and several samples show high contents of calcite in carbonate composition (Fig. 7). These evidences reveal that the paleolake was intermittently hydrologically open during middle–late Miocene. Additionally, the predominant closed lake conditions are also supported by the published stable isotope data from the outcrop sections in the western Qaidam basin. The stable isotopes from the Ganchaigou (Kent-Corson et al., 2009) and Youshashan (Rieser et al., 2009) Sections indicate high variations in the $\delta^{18}O$ values of the middle–late Miocene lacustrine marlstones (17 samples in the Ganchaigou Section, from −9.5‰ to −4.2‰; 6 samples in the Youshashan Section, from −9.1‰ to −4.7‰) and relatively high correlations between carbon and oxygen isotopes.

5.3. Paleoclimate change and its implications

The middle–late Miocene paleoclimatic history is investigated by combining the facies of subsurface drilling cores, the biomarkers of organic matter in the lake fine-grained sediments and the stable isotopes of lacustrine primary carbonates, and then the potential triggers for the climatic variations are discussed.

5.3.1. Evidence from facies and biomarkers

The facies study does not only suggest the shallowing lake water, but also indicates the increasing salinity during middle–late Miocene. The lake level decrease can be attributed to the output of the lake water or tectonic uplift, but the salinity increase should be due to relatively low precipitation/evaporation ratios, suggesting an intensified aridity over

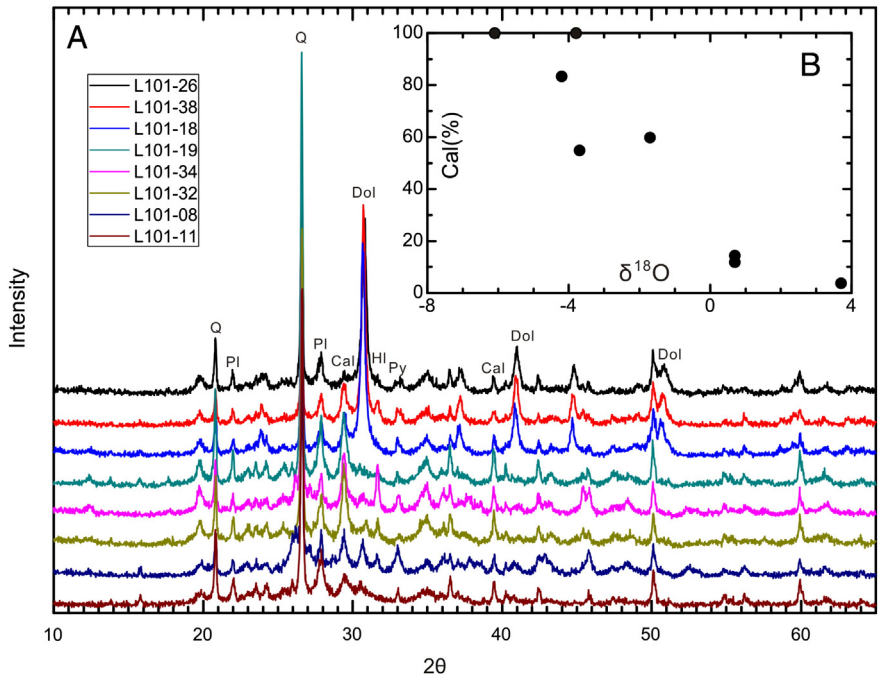

Fig. 7. XRD analysis results of selected samples (A) and the relation between $\delta^{18}O$ values and calcite proportions in carbonates (B). Q: quartz; Pl: plagioclase; cal: calcite; dol: dolomite; Hl: halite; Py: pyrite. The calcite proportions in carbonates were calculated based on the XRD analysis results.

time. The intensive evaporation and aridification are also supported by the frequent occurrence of primary evaporite minerals in the Facies 2 and 3, such as anhydrite, gypsum and halite (Figs. 3C, 4B, 7A).

Several biomarker proxies are considered as sensitive indicators of paleoclimate and thus can be used to reconstruct the paleoclimatic history. For example, the C_{27} or C_{29} n-alkanes have been thought to come from deciduous trees (Cranwell, 1973) while C_{31} or C_{33} n-alkanes have been proposed to come from grasses (Cranwell et al., 1987; Meyers and Ishiwatari, 1993; Xie et al., 2002; Zhang et al., 2006), therefore, the ratios such as C_{27}/C_{31}, $(C_{27} + C_{29})/(C_{31} + C_{33})$ and ACL values are often used to estimate changes in vegetation type and thus paleoclimate. Although the $>C_{27}$ n-alkanes are very low in our analyzed samples (see the preceding discussion), the results show that both C_{27}/C_{31} and $(C_{27} + C_{29})/(C_{31} + C_{33})$ ratios have decreasing trends and the ACL values have an increasing trend over time. This indicates the intensified aridity during middle–late Miocene. CPI values, which summarize the relative proportions of even-numbered and odd-numbered chain lengths in n-alkane distributions of geological samples, change with microbial reworking and diagenesis (Cranwell et al., 1987). The CPI values of geolipids can to some degree reflect paleoclimate because the rates of degradation and alteration differ under different climatic conditions (e.g. Zhou et al., 2005). Under a cold, dry climate, microbial activity is low and thus such conditions tend to yield high CPI values (e.g. Xie et al., 2004). In contrast, lower CPI values commonly result from accelerated microbial activity associated with a warm and wet climate (Zhou et al., 2005). The CPI values of the samples in this study have an increasing trend over time, implying increasingly cold and dry conditions during middle–late Miocene. This conclusion coincides with the previous results of chemical weathering evaluation (Jian et al., 2013a), pollen analysis (Wang et al., 1999; Miao et al., 2011) and sedimentological and geochemical analyses (Song et al., 2014).

5.3.2. Evidence from stable isotopes

The paleolake of the study area displayed hydrological closure with intermittently open conditions during middle–late Miocene, and the high fluctuations in $\delta^{18}O$ values (Fig. 8) were due to variable precipitation/evaporation ratios, in other words, residence time of the lake water and corresponding calcite proportions in carbonates (Fig. 7). This means that these $\delta^{18}O$ values cannot represent the isotopes of meteoric water. Hence, it may be inappropriate to investigate the paleoclimate change directly based on the $\delta^{18}O$ values. The samples, whose oxygen isotopes locate at the most negative end of the oscillations of $\delta^{18}O$ values, have the highest calcite contents (100% or nearly 100%, in carbonates). This implies an open lake condition where evaporation is minimal. Further these most negative data show surprising stability in Shang Youshashan and Shizhigou Formations (Fig. 8), with averages of −6.3‰ (n = 5, s.d. = 0.6‰) and −3.8‰ (n = 4, s.d. = 0.2‰), respectively. Based on this interpretation, it is obvious that a positive ~2.5‰ shift in $\delta^{18}O$ values occurred at ~10–8 Ma (the stratigraphic age is estimated on the base of typical magnetostratigraphy section in the Qaidam basin and the related stratigraphic correlation, see Fig. 1). Similar positive

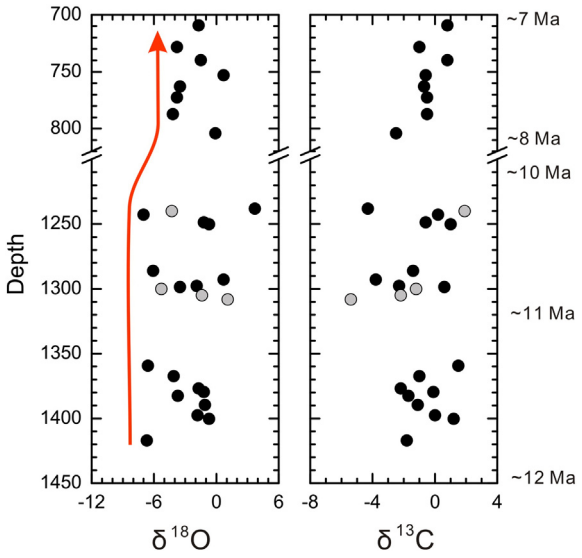

Fig. 8. Vertical variations of $\delta^{13}C$ and $\delta^{18}O$. This vertical evolution illustrates the data combination of samples from drilling cores of three wells, i.e., Wells Liang 101, Liang 5 and Liang 6, based on the high-resolution stratigraphic correlation. Note the data with black solid circles are from Well Liang 101. For the raw data, see Table 2.

shifts in $\delta^{18}O$ values can also be observed in adjacent areas. Zhuang et al. (2011a) found a positive shift in the northeastern Qaidam basin, starting around 12 Ma with a sharp increase around 10.7 Ma, while positive shifts in Linxia and Xuanhua basins in the northeastern corner of the Tibetan Plateau occurred at ~12–11 Ma (Dettman et al., 2003; Hough et al., 2011). In addition, steadily increasing oxygen isotopic trends were found in the Tarim basin during the Neogene (Kent-Corson et al., 2009). All of these findings suggest that the positive increase in $\delta^{18}O$ values was a regional change in the northern Tibetan Plateau. The surprising stability in the most negative oxygen isotopes (Fig. 8) suggests relatively stable climatic conditions before and after the positive shift, thus the most probable interpretation is a significant change in climate and/or in atmospheric circulation patterns in this region. Combining the explanations of facies and biomarker analysis results, the positive ~2.5‰ shift in $\delta^{18}O$ values is best explained by strengthened aridity in central Asia.

The $\delta^{18}O$ values of the northwest area (i.e. Xiaoliangshan area, this study) are consistently enriched relative to the northeast area (Huaitoutala section, Zhuang et al. (2011a)) in the Qaidam basin, although the positive shift extents are similar in these two areas. The enrichment of carbonate $\delta^{18}O$ values suggests a more arid condition in the west area relative to the east area. This also implies the hydrological separation during that time. Our study area displayed hydrological closure with intermittently open conditions, while the northeastern Qaidam basin was in open lake systems (Zhuang et al., 2011a). The hydrological separation was likely due to the distinct sedimentary environments and different drainages. The northeastern was characterized by distant alluvial fan and fluvial environments with lacustrine intervals, and the sediments were dominantly fed by the Qilian belt (Fang et al., 2007; Lu and Xiong, 2009; Zhuang et al., 2011a; Jian et al., 2013a,b), while the west area was dominated by semi-deep or shallow lacustrine environments, and the East Kunlun and Altun Mountains served as the predominant source areas (Rieser et al., 2009). The potential basin segments, which were indicated by the development of growth folds within the west and north areas (e.g. Wang et al., 2006; Yin et al., 2008a) at that time, might be another reason for the hydrological separation.

Generally, the lacustrine micritic carbonate C isotope can be influenced by the following factors: (1) photosynthesis and respiration within lake water; (2) CO_2 exchange between atmosphere and water; (3) isotopic composition of water feeding the lake and type of vegetation surrounding the lake; (4) CO_2 released during oxidation of organic matter (Leng and Marshall, 2004). In this study, the $\delta^{13}C$ values of the Shang Youshashan Formation samples have a wide range (Table 2), and the fluctuation is likely to be mainly attributed to the oxidation of organic matter and related CO_2 release. This can be explained as follows. As high $\delta^{18}O$ values indicate low precipitation/evaporation ratios, which probably lead to relatively shallow lake water intervals. In this condition, the organic matters in the bottom of lake, which have obviously low $\delta^{13}C$ values, can be oxidized to CO_2, resulting in low $\delta^{13}C$ values in the lacustrine carbonates. Photosynthesis may not be the major cause, because low $\delta^{13}C$ values need decreased photosynthesis (Talbot, 1990), which cannot be exist in the preceding conditions. The contribution of terrestrial plants should be minor, because of the relatively deep lake water during that time. However, the $\delta^{13}C$ values of the Shizigou Formation samples are relatively high and have small range, thus the fluctuation is probably due to the contribution of terrestrial plants (especially C4 plant (Cerling and Quade, 1993)) and photosynthesis. It is also supported by the shallowing lake water (Fig. 6), intensified aridity and the biomarker analysis results (Fig. 5). We only provide the potential interpretation, and further studies are needed to have a deeper understanding concerning the correlation between lacustrine carbonate carbon and oxygen isotopes in the Qaidam basin.

5.3.3. Controls on aridity

Late Cenozoic aridification in Central Asia has attracted much attention for decades. Several regional geological events are thought to be the key triggers, including the uplift of Tibetan Plateau, the retreat of the Paratethys and the global cooling. More and more studies agree that the arid climate was an integrated result of these factors. However, investigations based on different climatic proxies can provide different interpretations and conclusions, and it is hard to tell the absolute contribution ratios and which of these factors plays the major role.

The formation and uplift of the Himalayan–Tibetan system began about 50 Ma ago, and significant increases in altitude are thought to have occurred since middle–late Miocene (e.g. Harrison et al., 1992; Molnar, et al., 1993; Garzione et al., 2000a,2000b; Rowley et al., 2001). A growing body of investigations contend that the large and rapid elevation increases of this region led to changes of Indian and east Asian monsoons (e.g. Kutzbach et al., 1993; An et al., 2001; Miao et al., 2012), which then strengthened aridity in the Asian interior, including the Qaidam basin. The occurrence of the high-elevation Tibetan Plateau enhances Asian summer and winter monsoons and blocks the transfer of Indian Ocean-sourced air masses into Asian interior. Thus, the uplift of the Tibetan Plateau played a significant role in the aridification of the Qaidam basin during late Cenozoic (Kutzbach et al., 1993; An et al., 2001). Locally, thermochronological and tectono-sedimentological studies also supported the Miocene mountain-building and rapid uplift of the northern Tibetan Plateau. The (U–Th)/He and apatite fission track analysis of samples from the Altun Mountains (e.g. Jolivet et al., 2001; Sobel et al., 2001; Ritts et al., 2008) and East Kunlun (e.g. Chen et al., 2011; Duvall et al., 2013) showed that the rapid cooling had initiated by middle–late Miocene (about 15–10 Ma); seismic data of the western Qaidam basin indicated a local unconformity between the Xia Youshashan and Shang Youshashan Formations, suggesting an intensive uplift event in middle Miocene (Liu et al., 2007; Wang et al., 2010; Jian, 2013). In the Qilian Mountains, the fission-track analysis and (U–Th)/He thermochronological results on basement rocks supported the Miocene (~10 Ma) rapid uplift event (e.g. George et al., 2001; Zheng et al., 2010). The uplift event is also reinforced by the high-gradient depositional systems in the margin of the basin (Zhuang et al., 2011b; Jian, 2013) and an increase in sedimentation ratios (Fang et al., 2007; Lu and Xiong, 2009) since middle–late Miocene. The rapid uplift of the surrounding mountains resulted in the block of moisture transfer into the Qaidam basin and thus led to the increasing aridity.

The previous atmospheric general circulation model (AGCM) simulations illustrated that the Paratethys, which covered a large area of Central Asia during most of the Oligocene time (Ramstein et al., 1997), crucially influenced the climate. With the westward regression of the Paratethys, it could only occupy an area of the present Aral Sea, Caspian Sea and Black Sea and their surrounding regions (Ramstein et al., 1997) in middle–late Miocene (about 10 Ma). This retreat resulted in the absence of nearby moisture sources and thus shifted the Central Asian climate from temperate to continental conditions (Ramstein et al., 1997) and strengthened the East Asian monsoon (Zhang et al., 2007a, 2007b). The annual thermal amplitude increased to 30 °C or more, and the precipitation decreased significantly in this region (Ramstein et al., 1997). These changes significantly increased humidity in the monsoon areas and aridity in the northwestern China respectively.

Sporopollen studies of the western Qaidam basin, which indicated the decrease of thermophilic taxa and conifer percentages and the increase of xerophytic taxa percentages were synchronous since middle Miocene (e.g. Miao et al., 2011, 2013), advocated associating the arid conditions with climatic cooling. They contended that the Miocene global cooling could exert a significant influence on the aridification in Central Asia through reducing water vapor concentrations in the atmosphere. However, it might not be the dominant trigger for the positive ~2.5‰ shift in the $\delta^{18}O$ values. This can be explained as follows. It is true that decrease in temperature can lead to increase in the $\delta^{18}O$ values of precipitates in lakes, but for equilibrium carbonates, the isotope ratios increase by ~0.24‰ for each 1 °C decrease in temperature (Craig, 1965). This means a positive ~2.5‰ shift would require a rapid cooling of ~10 °C. However, during the middle Miocene climate cooling, the global

average temperature only dropped ~5 °C associated with the formation of the East Antarctic ice sheet (Zachos et al., 2001, 2008; Shevenell et al., 2004). Most stable isotope analysis results (e.g. Dettman et al., 2003; Hough et al., 2011; Zhuang et al., 2011a and this study) show that the aridification occurred at ~12–10 Ma, even later, whereas global cooling as documented in marine records, occurred prior to 14 Ma (e.g. Zachos et al., 2001; Molnar, 2004). In addition, the sporopollen records in the western Qaidam basin indicate the climatic cooling initiated by ~14 Ma (Miao et al., 2011, 2013).

6. Conclusion

This study combines facies, biomarker and carbonate stable isotope data of the middle–late Miocene sediments in the northwestern Qaidam basin, and yields the following conclusions concerning sedimentary environment, paleolake hydrology and paleoclimate change:

1) Three kinds of facies were identified, therein, gray–black laminated mudstone and marlstone (Facies 1) are likely to be formed in a semi-deep fresh to semi-brackish lake environment, while gray, yellowish massive mudstone, marlstone and siltstone (Facies 2) and yellowish massive sandstone (Facies 3) are probably produced in a shallow brackish lake environment. The vertical variation of facies suggests that the lake water became increasingly shallow and brackish over time.
2) Based on the stable isotopes and mineral compositions of lacustrine carbonate, it is suggested that the paleolake of the study area showed hydrological closure with intermittently open conditions during middle–late Miocene. The high fluctuations in $\delta^{18}O$ values and carbonate components are likely due to different precipitation/evaporation ratios. These $\delta^{18}O$ values of the northwest area are consistently enriched relative to the northeast area (e.g. Huaitoutala section, Zhuang et al. (2011a)) in the Qaidam basin, implying the hydrological separation and basin segment during that time.
3) The intensified aridity can be indicated by facies and related sedimentary environmental variations, biomarker proxies and oxygen isotope compositions. Abundant primary evaporite minerals in Facies 2 and 3 suggest the increasing salinity in the lake water; the variations of biomarker proxies, such as the decreasing C_{27}/C_{31} and $(C_{27} + C_{29})/(C_{31} + C_{33})$ values and the increasing ACL values, indicate more contributions of grasses and thus imply more arid conditions; the most negative end of the oscillations of the $\delta^{18}O$ values, which is considered as the indicator of minimal evaporation, displays stability in the Shang Youshashan and Shizigou Formations, respectively, and exhibits a positive ~2.5‰ shift. This significant shift is considered as a result of the intensified aridity and the change of air masses around 10–8 Ma ago.
4) It is suggested that the intensive aridification resulted from the integration of global cooling, high elevation of the Himalaya–Tibetan system (including the high mountain ranges around the basin) and the Paratethys retreat during middle–late Miocene, whereas the global cooling might not be the major trigger on the variation or shift of the stable isotopes of the lake carbonates.

Acknowledgments

We would like to thank Jun Cui of PetroChina Qinghai Oilfield Company for participating in the study. Shibiao Deng, Jiawei Tang and Rui Zhang are thanked for their help during the sampling. We appreciate Prof. Qianxiang Meng of Key Laboratory of Petroleum Resources Research, Institute of Geology and Geophysics, Chinese Academy of Sciences for his help in laboratory analysis. This work is supported by the (973) National Basic Research Program of China (Grant No. 2012CB214801), the Major National S&T Program of China (Grant No. 2011ZX05009-002-403, 2011ZX05004-004–005) and the grants from the PetroChina Qinghai Oilfield Company (Kantan-2011-Jishu-02). We are grateful to Katie Whitcombe for her significant efforts in improving the English language of the manuscript. The Editor Prof. Finn Surlyk and two anonymous reviewers provided constructive and thoughtful comments that improved this manuscript.

Appendix A. Supplementary data

Supplementary data to this article can be found online at http://dx.doi.org/10.1016/j.palaeo.2014.09.011.

References

An, Z., Kutzbach, J.E., Prell, W.L., Porter, S.C., 2001. Evolution of Asian monsoons and phased uplift of the Himalaya Tibetan plateau since late Miocene times. Nature 411, 62–66.
Bai, Y., Fang, X., Nie, J., Wang, Y., Wu, F., 2009. A preliminary reconstruction of the paleoecological and paleoclimatic history of the Chinese Loess Plateau from the application of biomarkers. Palaeogeogr. Palaeoclimatol. Palaeoecol. 271, 161–169.
Barnes, M.A., Barnes, W.C., 1978. Organic compounds in lake sediments. In: Lerman, A. (Ed.), Lakes: Chemistry, Geology, Physics. Springer-Verlag, Berlin, pp. 127–152.
Cerling, T.E., Quade, J., 1993. Stable carbon and oxygen isotopes in soil carbonates. In: Swart, P.K., Lohmann, K.C., McKenzie, J.A., Savin, S. (Eds.), Climate Change in Continental Isotopic Records. AGU Geoph. Monog 78, pp. 217–231.
Chen, X.H., McRivette, M.W., Li, L., Yin, A., Jiang, R.B., Wan, J.L., Li, H.J., 2011. Thermochronological evidence for multi-phase uplifting of the East Kunlun Mountains, northern Tibetan Plateau. Geol. Bull. China 30, 1647–1660 (in Chinese with English abstract).
Craig, H., 1965. The measurement of oxygen isotope palaeotemperatures. In: Tongiorgi, E. (Ed.), Stable Isotopes in Oceanographic Studies and Palaeotemperatures. Consiglio Nazionale delle Ricerche Laboratorio di Geologia Nucleare, Pisa, pp. 161–182.
Cranwell, P.A., 1973. Branched-chain and cyclopropanoid acids in a recent sediment. Chem. Geol. 11, 307–313.
Cranwell, P.A., 1984. Lipid geochemistry of sediments from Upton Broad, a small productive lake. Org. Geochem. 7, 25–37.
Cranwell, P.A., Eglinton, G., Robinson, N., 1987. Lipids of aquatic organisms as potential contributors to lacustrine sediments—II. Org. Geochem. 6, 513–527.
Dettman, D., Fang, X., Garzione, C., Li, J., 2003. Uplift-driven climate change at 12 Ma: a long [delta]^{18}O record from the NE margin of the Tibetan plateau. Earth Planet. Sci. Lett. 214, 267–277.
Ding, Z., Sun, J., Yang, S., Liu, T., 1998. Preliminary magnetostratigraphy of a thick eolian red clay-loess sequence at Lingtai, the Chinese Loess Plateau. Geophys. Res. Lett. 25, 1225–1228.
Drummond, C.N., Patterson, W.P., Walker, J.C.G., 1995. Climatic forcing of carbon–oxygen isotopic covariance in temperate-region marl lakes. Geology 23, 1031–1034.
Duan, Y., Wu, B., Xu, L., He, J., Sun, T., 2011. Characterisation of n-alkanes and their hydrogen isotopic composition in sediments from Lake Qinghai, China. Org. Geochem. 42, 720–726.
Duvall, A.R., Clark, M.K., Kirby, E., Farley, K.A., Craddock, W.H., Li, C., Yuan, D.-Y., 2013. Low-temperature thermochronometry along the Kunlun and Haiyuan Faults, NE Tibetan Plateau: evidence for kinematic change during late-stage orogenesis. Tectonics 32, 1190–1211.
Fang, X., Zhang, W., Meng, Q., Gao, J., Wang, X., King, J., Song, C., Dai, S., Miao, Y., 2007. High-resolution magnetostratigraphy of the Neogene Huaitoutala section in the eastern Qaidam Basin on the NE Tibetan Plateau, Qinghai Province, China and its implication on tectonic uplift of the NE Tibetan Plateau. Earth Planet. Sci. Lett. 258, 293–306.
Ficken, K.J., Li, B., Swain, D.L., Eglinton, G., 2000. An *n*-alkane proxy for the sedimentary input of submerged/floating freshwater aquatic macrophytes. Org. Geochem. 31, 745–749.
Garzione, C.N., Dettman, D.L., Quade, J., DeCelles, P.G., Butler, R.F., 2000a. High times on the Tibetan Plateau: paleoelevation of the Thakkhola graben, Nepal. Geology 28, 339–342.
Garzione, C.N., Quade, J., DeCelles, P.G., English, N.B., 2000b. Predicting paleoelevation of Tibet and the Himalaya from [delta]^{18}O vs. altitude gradients in meteoric water across the Nepal Himalaya. Earth Planet. Sci. Lett. 183, 215–229.
Gehrels, G., Yin, A., Wang, X., 2003a. Detrital-zircon geochronology of the northeastern Tibetan Plateau. Geol. Soc. Am. Bull. 115, 881–896.
Gehrels, G.E., Yin, A., Wang, X.F., 2003b. Magmatic history of the northeastern Tibetan Plateau. J. Geophys. Res. 108 (B9), 2423.
George, A., Marshallsea, S., Wyrwoll, K., Jie, C., Yanchou, L., 2001. Miocene cooling in the northern Qilian Shan, northeastern margin of the Tibetan Plateau, revealed by apatite fission-track and vitrinite-reflectance analysis. Geology 29, 939–942.
Graham, S.A., Chamberlain, C.P., Yue, Y., Ritts, B.D., Hanson, A.D., Horton, T.W., Waldbauer, J.R., Poage, M.A., Feng, X., 2005. Stable isotope records of Cenozoic climate and topography, Tibetan Plateau and Tarim Basin. Am. J. Sci. 305, 101–118.
Hanson, A.D., 1999. Organic Geochemistry and Petroleum Geology, Tectonics and Basin Analysis of Southern Tarim and Northern Qaidam Basins, Northwest China: Ph.D. Dissertation. Stanford University, Stanford, California, p. 388.
Harrison, T.M., Copeland, P., Kidd, W.S.F., Yin, A., 1992. Raising Tibet. Science 255, 1663–1670.
He, G., Tan, Y., Guan, P., Li, Y., Zhang, W., Du, B., 2008. Research on the Tertiary oil source in the northwest Qaidam basin. Nat. Gas Geosci. 19, 509–518 (In Chinese with English abstract).
Heermance, R.V., Pullen, A., Kapp, P., Garzione, C.N., Bogue, S., Ding, L., Song, P., 2013. Climatic and tectonic controls on sedimentation and erosion during the Pliocene–Quaternary in the Qaidam Basin (China). Geol. Soc. Am. Bull. 125, 833–856.

Hodell, D.A., Schelske, C.L., Fahnenstiel, G.L., Roberts, L.L., 1998. Biologically induced calcite and its isotopic composition in Lake Ontario. Limnol. Oceanogr. 43, 187–190.
Hough, B.G., Garzione, C.N., Wang, Z., Lease, R.O., Burbank, D.W., Yuan, D., 2011. Stable isotope evidence for topographic growth and basin segmentation: implications for the evolution of the NE Tibetan Plateau. Geol. Soc. Am. Bull. 123, 168–185.
Jian, X., 2013. Controls on Mesozoic and Cenozoic Sedimentary Evolution of the Northern Qaidam Basin: Tectonic and Climatic ImplicationsUnpub. Ph.D. dissertation Peking University, (In Chinese with English abstract).
Jian, X., Guan, P., Zhang, D.-W., Zhang, W., Feng, F., Liu, R.-J., Lin, S.-D., 2013a. Provenance of Tertiary sandstone in the northern Qaidam basin, northeastern Tibetan Plateau: integration of framework petrography, heavy mineral analysis and mineral chemistry. Sediment. Geol. 290, 109–125.
Jian, X., Guan, P., Zhang, W., Feng, F., 2013b. Geochemistry of Mesozoic and Cenozoic sediments in the northern Qaidam basin, northeastern Tibetan Plateau: implications for provenance and weathering. Chem. Geol. 360, 74–88.
Jolivet, M., Brunel, M., Seward, D., Xu, Z., Yang, J., Roger, F., Tapponnier, P., Malavieille, J., Arnaud, N., Wu, C., 2001. Mesozoic and Cenozoic tectonics of the northern edge of the Tibetan plateau: fission-track constraints. Tectonophysics 343, 111–134.
Kent-Corson, M.L., Ritts, B.D., Zhuang, G., Bovet, P.M., Graham, S.A., Chamberlain, C.P., 2009. Stable isotopic constraints on the tectonic, topographic, and climatic evolution of the northern margin of the Tibetan Plateau. Earth Planet. Sci. Lett. 282, 158–166.
Kutzbach, J.E., Prell, W.L., Ruddiman, Wm.F., 1993. Sensitivity of Eurasian climate to surface uplift of the Tibetan Plateau. J. Geol. 101, 177–190.
Last, W.M., 1990. Lacustrine dolomite—an overview of modern, Holocene, and Pleistocene occurrences. Earth Sci. Rev. 27, 221–263.
Leng, M.J., Marshall, J.D., 2004. Palaeoclimate interpretation of stable isotope data from lake sediment archives. Quat. Sci. Rev. 23, 811–831.
Li, H.-C., Ku, T.-L., 1997. $\delta^{13}C$–$\delta^{18}O$ covariance as a paleohydrological indicator for closed-basin lakes. Palaeogeogr. Palaeoclimatol. Palaeoecol. 133, 69–80.
Liu, T., 1985. Loess and the Environment. China Ocean Press, p. 215.
Liu, Y., Neubauer, F., Ge, X., Genser, J., Yuan, S., Li, W., Gong, Q., Chen, Y., 2007. Geochronology of the Altun fault zone and rising of the Altun mountains. Chinese J. Geol. 42, 134–146 (in Chinese with English abstract).
Lowenstein, T.K., Hardie, L.A., 1985. Criteria for the recognition of salt-pan evaporites. Sedimentology 32, 627–644.
Lu, H., Xiong, S., 2009. Magnetostratigraphy of the Dahonggou section, northern Qaidam Basin and its bearing on Cenozoic tectonic evolution of the Qilian Shan and Altyn Tagh Fault. Earth Planet. Sci. Lett. 288, 539–550.
Meyers, P.A., Benson, L.V., 1987. Sedimentary biomarker and isotopic indicators of the paleoclimatic history of the Walker Lake basin, western Nevada. Org. Geochem. 13, 807–813.
Meyers, P.A., Ishiwatari, R., 1993. Lacustrine organic geochemistry: an overview of indicators of organic matters sources and diagenesis in lake sediments. Org. Geochem. 20, 867–900.
Miao, Y., Fang, X., Herrmann, M., Wu, F., Zhang, Y., Liu, D., 2011. Miocene pollen record of KC-1 core in the Qaidam Basin, NE Tibetan Plateau and implications for evolution of the East Asian monsoon. Palaeogeogr. Palaeoclimatol. Palaeoecol. 299, 30–38.
Miao, Y., Herrmann, M., Wu, F., Yan, X., Yang, S., 2012. What controlled Mid–Late Miocene long-term aridification in Central Asia? — global cooling or Tibetan Plateau uplift: a review. Earth Sci. Rev. 112, 155–172.
Miao, Y.F., Fang, X.M., Wu, F.L., Cai, M.T., Song, C.H., Meng, Q.Q., Xu, L., 2013. Late Cenozoic continuous aridification in the western Qaidam Basin: evidence from sporopollen records. Clim. Past 9, 1863–1877.
Molnar, P., 2004. Late Cenozoic increase in accumulation rates of terrestrial sediment: how might climate change have affected erosion rates? Annu. Rev. Earth Planet. Sci. 32, 67–89.
Molnar, P., England, P., Joseph, M., 1993. Mantle dynamics, uplift of the Tibetan plateau and the Indian monsoon. Rev. Geophys. 31, 357–396.
Poynter, J.G., Farrimond, P., Brassell, S.C., Eglinton, G., 1989. Aeolian-derived higher-plant lipids in the marine sedimentary record: links with paleoclimate. In: Leinen, M., Sarnthein, M. (Eds.), Palaeoclimatology and Palaeometeorology: Modern and Past Patterns of Global Atmosphere Transport. Kluwer, pp. 435–462.
Ramstein, G., Fluteau, F., Besse, J., Joussaume, S., 1997. Effect on orogeny, plate motion and land–sea distribution on Eurasian climate change over the past 30 million years. Nature 386, 788–795.
Rieser, A.B., Bojar, A., Neubauer, F., Genser, J., Liu, Y., Ge, X.-H., Friedl, G., 2009. Monitoring Cenozoic climate evolution of northeastern Tibet: stable isotope constraints from the western Qaidam Basin, China. Int. J. Earth Sci. 98, 1063–1075.
Ritts, B.D., Yongjun, Y., Graham, S.A., Sobel, E.R., Abink, O.A., Stockli, D.F., 2008. From sea level to high elevation in 15 million years: uplift history of the northern Tibetan Plateau margin in the Altun Shan. Am. J. Sci. 308, 657–678.
Rowley, D.B., Pierrehumbert, R.T., Currie, B.S., 2001. A new approach to stable isotope-based paleoaltimetry: implications for paleoaltimetry and paleohypsometry of the High Himalaya since the Late Miocene. Earth Planet. Sci. Lett. 188, 253–268.
Ruskin, B.G., Jordan, T.E., 2007. Climate change across continental sequence boundaries: paleopedology and lithofacies of Iglesia Basin, northwestern Argentina. J. Sediment. Res. 77, 661–679.
Schieber, J., 2002. Sedimentary pyrite: a window into the microbial past. Geology 30, 531–534.
Shevenell, A.E., Kennett, J.P., Lea, D.W., 2004. Middle Miocene southern ocean cooling and Antarctic cryosphere expansion. Science 305, 1766–1770.
Shi, Y., Tang, M., Ma, Y., 1999. Linkage between the second uplifting of the Qinghai–Xizang (Tibetan) Plateau and the initiation of the Asian monsoon system. Sci. China. Ser. D 42, 303–312.
Sobel, E.R., Arnaud, N., Jolivet, M., Ritts, B.D., Brunel, M., 2001. Jurassic to Cenozoic exhumation history of the Altyn Tagh range, northwest China, constrained by $^{40}Ar/^{39}Ar$ and apatite fission track thermochronology. Geol. Soc. Am. Mem. 194, 247–267.
Song, C., Hu, S., Han, W., Zhang, T., Fang, X., Gao, J., Wu, F., 2014. Middle Miocene to earliest Pliocene sedimentological and geochemical records of climate change in the western Qaidam Basin on the NE Tibetan Plateau. Palaeogeogr. Palaeoclimatol. Palaeoecol. 395, 67–76.
Talbot, M.R., 1990. A review of the palaeohydrological interpretation of carbon and oxygen isotopic ratios in primary lacustrine carbonates. Chem. Geol. (Isot. Geosci. Sec.) 80, 261–279.
Talbot, M.R., 1994. Paleohydrology of the late Miocene Ridge basin lake, California. Geol. Soc. Am. Bull. 106, 1121–1129.
Talbot, M.R., Kelts, K., 1986. Primary and iagenetic carbonates in the anoxic sediments of lake Bosumtwi, Ghana. Geology 14, 912–916.
Tapponnier, P., Xu, Z., Roger, F., Meyer, B., Arnaud, N., Wittlinger, G., Yang, J., 2001. Oblique stepwise rise and growth of the Tibet Plateau. Science 294, 1671–1677.
Teranes, J.L., McKenzie, J.A., 2001. Lacustrine oxygen isotope record of 20th-century climate change in central Europe: evaluation of climatic controls on oxygen isotopes in precipitation. J. Paleolimnol. 26, 131–146.
Viso, A.-C., Pesando, D., Bernard, P., Marty, J.-C., 1993. Lipid components of the Mediterranean seagrass *Posidonia oceanica*. Phytochemistry 34, 381–387.
Wang, J., Wang, Y.J., Liu, Z.C., Li, J.Q., Xi, P., 1999. Cenozoic environmental evolution of the Qaidam Basin and its implications for the uplift of the Tibetan Plateau and the drying of central Asia. Palaeogeogr. Palaeoclimatol. Palaeoecol. 152, 37–47.
Wang, E., Xu, F.-Y., Zhou, J.-X., Wan, J., Burchfiel, B.C., 2006. Eastward migration of the Qaidam basin and its implications for Cenozoic evolution of the Altyn Tagh fault and associated river systems. Geol. Soc. Am. Bull. 118, 349–365.
Wang, L., Xiao, A., Gong, Q., Liu, D., Wu, L., Zhou, S., Lou, Q., Sun, X., 2010. The unconformity in Miocene sequence of western Qaidam Basin and its tectonic significance. Sci. China Earth Sci. 53, 1126–1133.
Wang, J., Fang, X., Appel, E., Song, C., 2012. Pliocene–Pleistocene climate change at the NE Tibetan Plateau deduced from lithofacies variation in the drill core SG-1, Western Qaidam Basin, China. J. Sediment. Res. 82, 933–952.
Xia, W., Zhang, N., Yuan, X., Fan, L., Zhang, B., 2001. Cenozoic Qaidam basin, China: a stronger tectonic inversed, extensional rifted basin. AAPG Bull. 85, 715–736.
Xie, S., Wang, Z., Wang, H., Chen, F., An, Z., 2002. Grassy vegetation since the last interglacial in the Loess Plateau: the molecular fossil record. Sci. China Ser. D Earth Sci. 45, 53–63.
Xie, S., Chen, F., Wang, Z., Wang, H., Gu, Y., Huang, Y., 2003. Lipid distributions in loess-paleosol sequences from northwest China. Org. Geochem. 34, 1071–1079.
Xie, S., Nott, C.J., Avsejs, L.A., Maddy, D., Chambers, F., Evershed, R.P., 2004. Molecular and isotopic stratigraphy in an ombrotrophic mire for palaeoclimate reconstruction. Geochimica et Cosmochimica Acta 68, 2849–2862.
Yin, A., Harrison, T.M., 2000. Geologic evolution of the Himalayan–Tibetan orogen. Annu. Rev. Earth Planet. Sci. 28, 211–280.
Yin, A., Rumelhart, P.E., Butler, R.E., Cowgill, E., Harrison, T.M., Foster, D.A., Ingersoll, R.V., Zhang, Q., Zhou, X.-Q., Wang, X.-F., Hanson, A., Raza, A., 2002. Tectonic history of the Altyn Tagh fault system in northern Tibet inferred from Cenozoic sedimentation. Geol. Soc. Am. Bull. 114, 1257–1295.
Yin, A., Dang, Y., Wang, L., Jiang, W., Zhou, S., Chen, X., Gehrels, G.E., McRivette, M.W., 2008a. Cenozoic tectonic evolution of Qaidam basin and its surrounding regions (part 1): the southern Qilian Shan-Nan Shan thrust belt and northern Qaidam basin. Geol. Soc. Am. Bull. 120, 813–846.
Yin, A., Dang, Y., Zhang, M., Chen, X., McRivette, M.W., 2008b. Cenozoic tectonic evolution of the Qaidam basin and its surrounding regions (part 3): structural geology, sedimentation, and regional tectonic reconstruction. Geol. Soc. Am. Bull. 120, 847–876.
Yue, Y., Liou, J.G., 1999. Two-stage evolution model for the Altyn Tagh fault, China. Geology 27, 227–230.
Yue, Y., Ritts, B.D., Graham, S.A., Wooden, J.L., Gehrels, G.E., Zhang, Z., 2003. Slowing extrusion tectonics: lowered estimate of post-Early Miocene slip rate for the Altyn Tagh fault. Earth Planet. Sci. Lett. 217, 111–122.
Zachos, J.C., Pagani, M., Sloan, L., Thomas, E., Billups, K., 2001. Trends, rhythms, and aberrations in global climate 65 Ma to present. Science 292, 686–693.
Zachos, J.C., Gerald, R.D., Richard, E.Z., 2008. An early Cenozoic perspective on greenhouse: warming and carbon-cycle dynamics. Nature 451, 279–283.
Zhang, Z., Zhao, M., Eglinton, G., Lu, H., Huang, C., 2006. Leafwax lipids as paleovegetational and paleoenvironmental proxies for the Chinese Loess Plateau over the last 170 kyr. Quat. Sci. Rev. 25, 575–594.
Zhang, Z., Wang, H., Guo, Z., Jiang, D., 2007a. Impacts of tectonic changes on the reorganization of the Cenozoic paleoclimatic patterns in China. Earth Planet. Sci. Lett. 257, 622–634.
Zhang, Z., Wang, H., Guo, Z., Jiang, D., 2007b. What triggers the transition of palaeoenvironmental patterns in China, the Tibetan Plateau uplift or the Paratethys Sea retreat? Palaeogeogr. Palaeoclimatol. Palaeoecol. 245, 317–331.
Zhang, C., Wang, Y., Li, Q., Wang, X., Deng, T., Tseng, Z.J., Takeuchi, G.T., Xie, G., Xu, Y., 2012. Diets and environments of late Cenozoic mammals in the Qaidam Basin, Tibetan Plateau: evidence from stable isotopes. Earth Planet. Sci. Lett. 333, 70–82.
Zheng, D., Clark, M., Zhang, P., Zheng, W., Farley, K., 2010. Erosion, fault initiation and topographic growth of the North Qilian Shan (northern Tibetan Plateau). Geosphere 6, 937–941.
Zhou, W., Xie, S., Meyers, P.A., Zheng, Y., 2005. Reconstruction of late glacial and Holocene climate evolution in southern China from geolipids and pollen in the Dingnan peat sequence. Org. Geochem. 36, 1272–1284.
Zhuang, G., Hourigan, J.K., Koch, P.L., Ritts, B.D., Kent-Corson, M.L., 2011a. Isotopic constraints on intensified aridity in Central Asia around 12 Ma. Earth Planet. Sci. Lett. 312, 152–163.
Zhuang, G., Hourigan, J.K., Ritts, B.D., Kent-Corson, M.L., 2011b. Cenozoic multiple-phase tectonic evolution of the northern Tibetan Plateau: constraints from sedimentary records from Qaidam basin, Hexi Corridor, and Subei basin, northwest China. Am. J. Sci. 311, 116–152.